

AMERICAN UNIVERSITY OF BEIRUT

DETERMINATION OF THE EVAPORATION COEFFICIENT OF
SECONDARY ORGANIC AEROSOLS FROM GASOLINE
ENGINE EXHAUST

by
MOHAMAD AHMAD BAASSIRI

A thesis
submitted in partial fulfillment of the requirements
for the degree of Master of Engineering in Mechanical Engineering
to the Department of Mechanical Engineering
of the Faculty of Engineering and Architecture
at the American University of Beirut

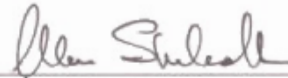
Beirut, Lebanon
May 2014

AMERICAN UNIVERSITY OF BEIRUT

DETERMINATION OF THE EVAPORATION COEFFICIENT OF
SECONDARY ORGANIC AEROSOLS FROM GASOLINE
ENGINE EXHAUST

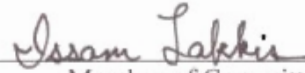
by
MOHAMAD AHMAD BAASSIRI

Approved by:



Dr. Alan Shihadeh, Professor
Department of Mechanical Engineering

Advisor



Dr. Issam Lakkis, Associate Professor
Department of Mechanical Engineering

Member of Committee



Dr. Fouad Azizi, Assistant Professor
Department of Chemical Engineering

Member of Committee

Date of thesis/dissertation defense: May 07, 2014

ACKNOWLEDGMENTS

I am grateful to my advisor, Prof. Alan Shihadeh, for his selfless time and support. Apart from his wide knowledge and exceptional expertise, his sense of humor and the confidence he used to give me throughout my research experience were sometimes all that kept me going. His guidance that never lacked a friendly attitude and his encouragement made a real difference in my academic skills.

My sincere recognition goes to Dr. Fouad Azizi and Dr. Issam Lakkis for being members on my thesis committee board. Their valuable feedback and comments really contributed to the quality of this work and boosted my performance. I also acknowledge Mr. Joseph Nassif and his working team for their technical support in building up the setup of my project.

To the Aerosol Lab group, or family as I love to call them, I extend my deep gratitude. This work wouldn't have been accomplished without the help of Rola Selman, who always made the flow of work easier through her wise management, and that of Nareg Karaoghlanian whose assistance and expertise added a lot to my experience. A special appreciation goes to my colleague Zainab Balhas with whom I shared the details of all the stress and pitfalls as well as success, and to Soha Talih for her consistent eagerness to provide helpful tips and share her research experience with me. Many thanks also go to Sara Jaber for being a very patient mentor and a supportive friend at the beginning of the work.

I would like to express my respect and thankfulness to all of my friends with whom I discussed every step throughout my graduate studies. I have no words to thank all of you Hussein Maanieh, Khaled Abu Hweij, Ayman Hijazi, Abdulrahman Dalibalta, Mohamad Kanaan, and Mohamad Mirhi for your inspiring tips and ideas.

I send my heartiest thanks to my parents whose unconditional support is the reason why I have reached this stage of the work where I can talk about my success. I am grateful to my father for the long conversations we used to share over the phone from KSA to discuss my future plans, and to my mother for the food she used to send me while on campus and for her daily phone calls just to make sure everything was going well with me. I shall thank my brother and sister for bearing with me as I kept on demanding for their help throughout my stay at AUB. I also owe a great deal of thanks to my cousins and relatives for their supportive words and for making me feel they are proud of what I'm doing.

AN ABSTRACT OF THE THESIS OF

Mohamad Ahmad Baassiri for Master of Engineering
Major: Mechanical Engineering

Title: Determination of the Evaporation Coefficient of Secondary Organic Aerosols from Gasoline Engine Exhaust

Organic aerosols constitute a major fraction of particle pollutants in the atmosphere, and they exert important influences on human health and global climate. When predicting concentrations of organic aerosols (OA) in the atmosphere, regional air quality models commonly assume that gas-particle partitioning is rapid, and that therefore semi-volatile species closely follow thermodynamic equilibrium partitioning between the condensed and vapor phases. Based on recent evidence from single-particle studies that secondary organic aerosols (SOA) exist in a glassy, amorphous state for which mass transfer is intrinsically slow compared to atmospheric time scales, the assumption that OA is well-described by equilibrium thermodynamics has been called into question. In this study, the evaporation kinetics of an ensemble of SOA nanoparticles is observed when they are heated to 40 °C in a constant temperature, atmospheric pressure flow tube. In particular, particle volume changes are tracked in time, and the observations are fitted to a theoretical model of particle evaporation in order to obtain the effective evaporation coefficient. The evaporation coefficient describes the rate of evaporation relative to the maximum theoretical rate of evaporation defined by kinetic theory of gases. SOA was generated by photo-oxidizing diluted (5000:1) exhaust from a single-cylinder gasoline engine. Investigated particle mass loadings spanned a range from 18 $\mu\text{g}/\text{m}^3$ to 40 $\mu\text{g}/\text{m}^3$. It was found that particle evaporation kinetics were well described by Maxwell's equation, with effective evaporation coefficients approaching unity. These results indicate that in the atmosphere anthropogenic SOA attain phase equilibrium on time scales approaching minutes or tens of minutes in extreme cases, and can generally be treated as continuously in thermodynamic equilibrium for regional air quality models.

CONTENTS

ACKNOWLEDGMENTS	v
ABSTRACT.....	vi
LIST OF ILLUSTRATIONS.....	x
LIST OF TABLES.....	xi
Chapter	
I. INTRODUCTION.....	1
II. THEORY.....	8
A. Single Particle Evaporation.....	8
B. Evaporation of an Aerosol in a Flow Tube.....	11
C. Evaporation of a Multi-component Aerosol.....	13
D. The Phase Equilibration Method.....	14
III. MATERIALS AND METHODS	17
A. Experimental Setup	17
1. The Engine and the Exhaust System.....	18
2. The Rotating Disk Diluter.....	19
3. The PAM Chamber and the Ultra Violet (UV) Lamp.....	19

4. The Thermo-denuder	20
B. Procedure	20
C. Experimental Conditions	22
D. Data Analysis.....	23
E. Assumptions Validation.....	26
F. Uncertainty Analysis	27
IV. RESULTS	28
A. SOA Generation	28
B. Particle Size Distribution	29
C. Equilibration Profile	31
D. Effective Evaporation Coefficient	33
V. DISCUSSION AND ANALYSIS	34
A. SOA Gas-particle Particle Partitioning	34
B. Effect of Evaporation Coefficient.....	35
C. Effect of Temperature.....	37
D. Limitations.....	38
E. Recommendations.....	38
VI. CONCLUSION	40
BIBLIOGRAPHY	41

ILLUSTRATIONS

Figure	Page
1: Atmospheric Aerosols	2
2: Formation Mechanisms of SOA in the Atmosphere	4
3: An Example of the Equilibration Profile.....	15
4: Experimental Setup for SOA Generation and Equilibration Profile Measurement	18
5: Simulations illustrating the effect of incorporating the Kelvin factor.	27
6: Evolution of SOA Mass Concentration inside the PAM Chamber (typical results).....	28
7: US and DS Size Distributions for Experiments 1 Through 5	30
8: Dimensional Equilibration Profiles for 5 Experiments Having Different Initial Loadings	32
9: Non-dimensional Equilibration Profiles for the 5 Experiments.....	32
10: Best Possible Fit for Equilibration Process based on $\alpha=10^{-4}$	36
11: Best Possible Fit for Equilibration Process based on $\alpha=0.01$	36
12: Temperature Effect on Maximum Change in Particles Volume through the TD	37

TABLES

Table	Page
1: Parameters of Equation 32	24
2: Parameters of Table 1	25
3: Size Distribution Characteristics	29
4: Chamber Temperature, Rh, and Mass Loading for Each Experiment	29
5: Critical Parameters and Obtained Evaporation Coefficients.....	33

CHAPTER I

INTRODUCTION

Atmospheric aerosols play a vital role in air quality on regional and global scales and are related to most influential environmental processes (Seinfeld and Pandis 2012). Due to their ability to scatter and absorb solar radiation, atmospheric aerosols can alter the solar energy fluxes and, therefore, have a direct impact on the global climate (Hallquist et al. 2009). Atmospheric aerosols can also indirectly influence the climate by constituting cloud condensation nuclei (CCN) and hence, contributing to cloud formation and modifying the microphysical properties of clouds as well as their lifetime (Haywood and Boucher 2000). The impact of atmospheric aerosols extends further to touch human life and public health. Submicron and microscopic aerosols can travel deep into the lungs and may penetrate the blood-gas barrier of the respiratory tract and accumulate in various organs (Pöschl 2005). Exposure to high concentrations of atmospheric aerosols can damage immunological, cardiovascular, and nervous systems (Pöschl 2005). Therefore, policies have been implemented to regulate emissions in order to limit their effects on health and environment. Air quality modeling has been a powerful tool used to assess the efficacy of these policies and to update related legislation (Chang and Hanna 2004). In short, air quality models convert pollutant emissions to air concentration values and use these predicted values to determine whether or not a certain policy does a good job in improving air quality (Williams et al. 2011).

In general, ambient aerosols include inorganic and organic aerosols (OA) in addition to water (Shiraiwa et al. 2013), with OA accounting for the major share among other species on a mass basis (Saxena et al. 1995). OA can be classified into volatile, non-volatile, and semi-

volatile organic aerosols (SVOA). SVOA are generally characterized by constant re-partitioning between the gaseous phase and the particle phase in response to changes of temperature, relative humidity, and concentrations (Chow et al. 1994). Any aerosol present in the atmosphere with more than 1% of its mass capable of inhabiting both the condensed and the vapor phase is defined as an SVOA (Donahue et al. 2006). SVOA are the most abundant type of ambient OA, and they can be emitted directly as so-called “primary organic aerosols” (POA) or formed in the atmosphere from gaseous precursors, in which case they are referred to as “secondary organic aerosols”, or SOA (Seinfeld and Pandis 2012). SVOA is largely SOA in origin (Robinson et al. 2007). SOA precursors can be biogenic (e.g. terpenes from pine trees), or anthropogenic (e.g. engine exhaust) (Pun et al. 2002). When these precursors are oxidized during atmospheric aging processes, they yield products with sufficiently low vapor pressures that they can condense into the particulate phase (Kanakidou et al. 2005).

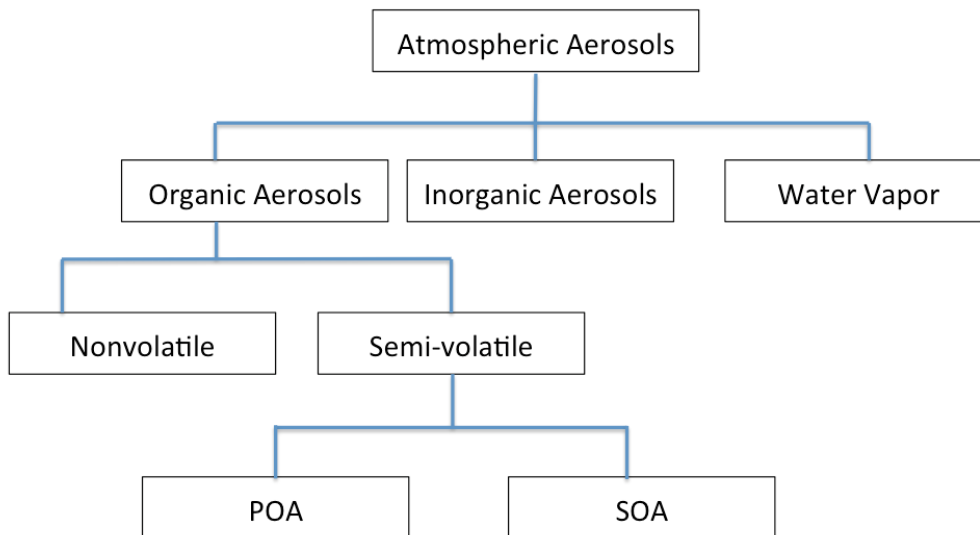


Figure 1: Atmospheric Aerosols

This transformation into the particulate phase may occur through condensation onto other POA by absorptive or adsorptive partitioning, or through homogeneous nucleation (Kanakidou et al. 2005). Gaseous precursors are oxidized by species like hydroxyl radicals (OH), ozone O₃, and nitrate radical (NO₃) to form larger molecules that can partition into the particle phase (Seinfeld and Pandis 2012). For anthropogenic SOA, the primary oxidizing agent is hydroxyl (OH) (Ziemann and Atkinson 2012). Equations (1) and (2) show how hydroxyl radicals could be formed, while equations (3) and (4) show how ozone is formed again after being dissociated (Seinfeld and Pandis 2012):



where hv is a high energy source, typically ultraviolet light, that attacks ozone to split it into an oxygen molecule and another oxygen atom with an electron in an excited state O(1D). This O(1D) attacks water vapor molecules to yield hydroxyl radicals. These hydroxyl radicals in turn oxidize organic gaseous precursors leading eventually to SOA formation. This process is often referred in the literature to as “aging”, and its steps are illustrated in Figure 2 below.

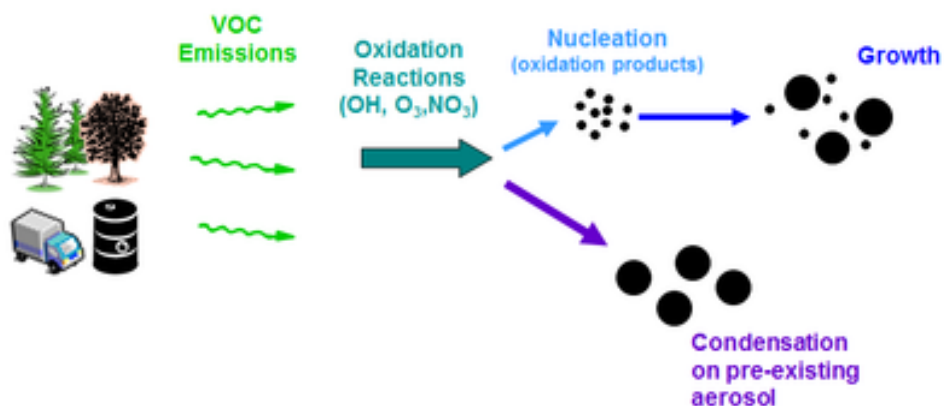


Figure 2: Formation Mechanisms of SOA in the Atmosphere

One of the key issues in predicting atmospheric SOA concentrations is how to model their gas-particle partitioning process (Henze et al. 2008), given the complexity and uncertainty of the SOA composition (Gordon et al. 2013). In fact, very little is known about the chemical composition of SOA, and crude thermodynamic property parameterizations are normally invoked in regional air quality models to compute gas-particle partitioning behavior. Regardless of the thermodynamic parameterizations used, a widely invoked model is the absorption model postulated by (Pankow 1994), in which it is assumed that partitioning occurs in an absorptive, well-mixed, organic matter phase (Pankow 1994). Pankow's absorptive partitioning model is standard in regional air quality models, which assume that atmospheric time scales are large compared to time scales of gas-particle partitioning kinetics. That is, it is assumed that gas-particle partitioning can reach to equilibrium within minutes which is a short timescale compared to the timescales of ambient aerosols residence within the atmosphere (hours to days) (Seinfeld and Pandis 2012). This allows treatment of SOA in the atmosphere using equilibrium thermodynamics alone without including information about the detailed evaporation kinetics (Pankow and Barsanti 2009). In that sense, the model predicts the fraction of organic matter that

will be in the particle phase after equilibrium is achieved in the atmosphere. So, the accuracy of predictions of regional air quality models depends on the validity of the assumption that SOA achieves phase equilibrium within atmospheric timescales.

The assumption that SOA achieves thermodynamic equilibrium in atmospheric timescales has been questioned by recent studies on SOA evaporation kinetics where an alternative model has been proposed (Vaden et al. 2011; Cappa and Wilson 2011) in which particle phase change is thought to be limited by mass transfer resistances due to particles being in an amorphous solid-state (Virtanen et al. 2010; Zobrist et al. 2008). Vaden et al. (2011) investigated evaporation kinetics of laboratory generated biogenic SOA at room temperature and based on observed slow evaporation rates, concluded that atmospheric partitioning of SOA is always mass transfer rate limited. Using photoionization mass spectrometry, Cappa and Wilson (2011) measured the evolution of composition of biogenic SOA upon heating and suggested that SOA evaporation does not follow absorptive partitioning theory. As a result, they argued, regional air pollution models require a new framework for gas-particle partitioning. When interpreting their measurements the authors of these studies assumed that the thermodynamic properties (e.g. volatility distributions), derived from earlier smog chamber experiments (Pathak et al. 2007) were applicable. Using these earlier reported thermodynamic data, the authors found that the observed particle evaporation kinetics were consistent with mass evaporation coefficients (α) of the order 10^{-2} to 10^{-4} , indicating extreme intrinsic mass transfer resistance. They found that SOA partitioning is slow relative to atmospheric time scales. More recently, Perraud et al. (2012) examined the condensational growth of biogenic SOA and compared the uptake of organic nitrates in their system to that predicted by a kinetic model. Results revealed that the formation did not follow the pathway predicted by absorptive partitioning theory, and

that a kinetically limited growth / evaporation mechanism best fits their data (Perraud et al. 2012).

Interestingly, smog chamber studies on formation mechanisms of SOA have revealed formation of extremely low volatility compounds, or oligomers, upon aging (Hall IV and Johnston 2011; Tolocka et al. 2004). It has been argued that recent reports of slow SOA evaporation kinetics may simply reflect that these recent studies have not accounted for oligomerization and therefore relied on incorrect thermodynamic data to compute theoretical evaporation rates. Indeed, a recent study by Saleh et al. (2013) of biogenic SOA evaporation kinetics, using a novel method which does not depend on prior knowledge of thermodynamic properties, found that biogenic SOA was well described by a well-mixed absorptive partitioning process with characteristic α in the range 0.1-1.

Mass transfer parameters affecting evaporation rate of an aerosol particle are diffusion coefficient (D) of particles in the surrounding gases and the evaporation coefficient (α). α , sometimes also referred to as the mass accommodation coefficient, is the ratio of the actual molecular flux from a surface relative to the maximum theoretical flux predicted by kinetic theory. Values less than unity indicate an interfacial mass transfer resistance other than gas phase diffusional resistance. It has become customary to lump all intra-particle and interfacial mass transfer resistances other than gas phase diffusion into an “effective” empirically measured α . Values close to unity indicate that molecular flux is well described by the diffusion equation (i.e. diffusional resistance in the gas phase limits flux), while values far less than unity represent intrinsic mass transfer limitations within the particle or at its surface. α is therefore a useful construct as an index of condensed phase mass transfer limitations.

Thesis Objective

While biogenic SOA precursors are often uncontrollable because they are of natural origin, anthropogenic SOA precursors are of known origins that are amenable to policy interventions. One of the most important anthropogenic precursors for SOA formation is “aromatic hydrocarbons”, released principally from automobile exhaust emissions (Odum et al. 1997). Hence, accurately predicting their concentrations in the atmosphere is central to the reliability of advanced air quality models. Recent studies have reported sluggish kinetics of SOA gas-particle equilibration and attributed this to intra-particle mass transfer inhibition. If these findings are correct, a rethinking of atmospheric pollution models may be necessary. We postulate that previous conclusions regarding slow evaporation rates may simply reflect low volatility rather than extreme mass transfer resistance. In this work, we will investigate the dynamics of gas-particle partitioning of SOA formed by oxidation of real gasoline engine exhaust, without making any assumption about the vapor pressure of the aerosol. Using the phase equilibration approach, the apparent evaporation coefficient of the formed SOA will be determined. Specific objectives of this thesis include:

1. Developing an SOA generation system for diluted engine exhaust emissions using the “Potential Aerosol Mass” approach of (Kang et al. 2007).
2. Developing an operating protocol to generate SOA with atmospherically relevant concentrations and size distributions
3. Developing a heated flow tube setup for executing the Phase Equilibration Method (Saleh et al. 2011).
4. Determining the effective α of engine exhaust SOA.

CHAPTER II

THEORY

A. Single Particle Evaporation

An aerosol is a system of particles suspended in the gaseous phase of these particles, or vapor, as well as other gases like air. When the vapor concentration at a particle's surface (C_s) is equal to that far from the surface, the aerosol is said to be in phase equilibrium. When C_s is greater or less than the surrounding vapor concentration, evaporation or condensation phase change occurs from/to the particles, respectively. The rate of evaporation or condensation depends on the length scales involved.

In the continuum regime, where the particle diameter is much larger than the mean free path (MFP) of the randomly colliding molecules of surrounding gas, the mass flux of vapor leaving a single particle is given by Fick's law of diffusion as:

$$j_c = -D \frac{dC}{dr} \quad (5)$$

Where j_c is the rate of mass flux of vapor in $\text{kg}/(\text{m}^2 \cdot \text{sec})$, D is the diffusion coefficient of the droplet in air in (m^2/sec) , C is the mass concentration of the vapor in the air in (kg/m^3) , and r is the radius of the droplet in (m).

Multiplying equation (5) by the surface area of the spherical particle gives:

$$I = -4\pi r^2 D \frac{dC}{dr} \quad (6)$$

Where I is the rate of mass transfer in kg/sec . Therefore, another representation of I would be:

$$I = -\frac{dm_p}{dt} \quad (7)$$

Where the negative sign represents the direction of the transfer of mass away from the droplet surface, and where units of I are still kg/sec.

From (6), we can write:

$$\frac{dC}{dr} = \frac{-I}{4\pi r^2 D} \quad (8)$$

Integrating Eq 8 from the surface of the droplet to $r = \infty$, we obtain:

$$C_s - C_\infty = \frac{I}{4\pi r D} \quad (9)$$

Hence,

$$I = 2\pi d_p D (C_s - C_\infty) \quad (10)$$

Equation (10) is commonly known as the Maxwell Equation (Maxwell 1890).

Substituting equation (10) in (7), we get the equation that governs the rate of change of mass of a droplet in the continuum regime:

$$\frac{dm_p}{dt} = -2\pi d_p D (C_s - C_\infty) \quad (11)$$

In the free-molecular regime, or the kinetic regime, where the particle's diameter is much smaller than the MFP of the surrounding gas, the transfer of vapor molecules from the particle depends on random molecular collisions rather than diffusion. The molecular flux would then be a function of the particle's diameter (d_p), number of molecules (N), average molecular speed (\bar{C}_A), and the "evaporation coefficient, α " as shown in Eq 12 (Moore 1962):

$$j_K = -\pi d_p^2 \frac{N}{4} \bar{C}_A \alpha (C_s - C_\infty) \quad (12)$$

The concept of the evaporation coefficient dates back to Maxwell (1859) and it is defined as the ratio of the actual molecular flux leaving the surface of a particle to the maximum molecular flux predicted by the kinetic theory of gases. There are a number of reasons that α may not be unity. One of them is that the molecules leaving the particle surface may not have a

Maxwell-Boltzmann velocity distribution (Hinds 2012). Another reason that α may be less than unity for a given aerosol system is that several surface and bulk interior effects can limit the rate at which molecules can desorb from the particle interface (Somorjai and Lester 1967).

Between the continuum regime and the kinetic regime is the transition regime, for which the ratio of the gas MFP to the particle's radius falls in a range of the order of unity. This is elucidated by the Knudsen number defined as $Kn=2\lambda/d_p$ where λ is the MFP of the surrounding gas. Atmospheric SOA generally inhabits the transition regime, i.e. particles ranging from a few nanometers to hundreds of nanometers, for which there is no direct expression that describes the molecular flux (Rader et al. 1987).

Hence, to correct for non-continuum effects, an interpolation factor $F(Kn,\alpha)$ is introduced to Eq 7. Several expressions have been used to interpolate between the continuum and the kinetic regimes, only one of which explicitly accounts for differing molecular weights of the evaporating species and air. This factor is known as the Sitarski-Nowakowski factor (Sitarski and Nowakowski 1979)

To account for curvature effect on the surface vapor concentration, C_s in equation (12) should be multiplied by the Kelvin correction factor defined as:

$$K = \exp\left(\frac{4\sigma M_B}{\rho_p T d_p}\right) \quad (13)$$

Where ρ_p is the particle density and σ is the surface tension at the droplet surface. The fact that curvature limits the number of molecules available at the surface leads to enhancement of the overall energy required for molecules to leave the particle. Hence, the surface concentration required to achieve equilibrium (i.e. saturation concentration) is enhanced by a factor of K , which is greater than unity as shown in (13).

Therefore, the governing equation of the mass transfer rate from a particle's surface to air becomes:

$$\frac{dm_p}{dt} = -2 \cdot \pi \cdot d_p \cdot D \cdot F(\text{Kn}, \alpha) (K \cdot C_{\text{sat}} - C_g) \quad (14)$$

Where C_{sat} and C_g has respectively replaced C_s and C_∞ . With the volume of a spherical droplet being: $V = \frac{\pi d_p^3}{6}$ and with the mass being: $m = \rho_p V$, equation of rate of change of particle's diameter can be derived from Eq 14 to give:

$$\frac{d d_p}{dt} = \frac{4 \cdot D \cdot F(\text{Kn}, \alpha) (K \cdot C_{\text{sat}} - C_g)}{\rho_p \cdot d_p} \quad (15)$$

As will be illustrated in a later section, the evaporation coefficient has a direct effect on mass transfer rate along with the diffusion coefficient, particle size, and number concentration. However, while the diffusion coefficient can be determined with good confidence (e.g. Chapman-Enskog Formula) (Reid et al. 1987), and particle size and number concentration can be measured, the evaporation coefficient remains the only uncertain parameter. With no reliable formulas to be used, a long history of controversy, and widely spanned suggested values, the only way of estimating the evaporation coefficient is experimentation (Davis and Schweiger 2002).

B. Evaporation of an Aerosol in a Flow Tube

As an aerosol initially at thermodynamic equilibrium flows through a heated tube, heat will be transferred from the tube wall to the gaseous bulk where the particles are suspended, and then from the bulk to the particles. As the particles are heated, their saturation vapor pressure increases creating a pressure gradient that acts as a driving potential for evaporation of these particles.

Assuming a plug flow inside the tube and neglecting wall losses, the equation governing gas concentration inside the thermo-denuder can be derived from mass conservation law to be:

$$\frac{dC_g}{dt} = -N \frac{dm_p}{dt} \quad (16)$$

Where C_g is the gas phase concentration, and N is the number concentration of particles. This equation states that the vapor concentration in the aerosol is changed by vapor being generated due to particles evaporation, or by vapor being lost due to condensation into the particles surfaces. In other words, loss in particle mass is translated as a gain in the gas phase concentration.

Substituting Eq 14 in Eq 16 gives the “equilibration profile equation”, which governs the rate at which an aerosol system approaches phase equilibrium:

$$\frac{dC_g}{dt} = 2 \cdot \pi \cdot d_p \cdot ND \cdot F(K \cdot C_{sat} - C_g) \quad (17)$$

The driving potential mentioned in the beginning of this section appears as the last term in Eq 17 suggesting that the aerosol will keep evaporating until the gas concentration is equal to the product of the Kelvin factor and the saturation concentration.

Eq 17 applies for a mono-disperse aerosol, i.e. an aerosol whose particles have the same diameter. Yet, this equation can be extended so that it can be used for a poly-disperse aerosol, i.e. an aerosol of various particles diameters. This can be done using the so-called “condensation-sink diameter”, the concept of which has been introduced by (Lehtinen et al. 2003).

The condensation-sink diameter is a moment average diameter of a mono-disperse aerosol that would yield the same net evaporation rate as the poly-disperse aerosol being represented (Lehtinen et al. 2003). It is given by the following formula:

$$d_{cs} = \left(\frac{\sum_i^n N_i d_p^a}{\sum_i^n N_i} \right)^{1/a} \quad (18)$$

where “a” is an exponent that varies between 1 for the continuum regime, and 2 for the non-continuum regime.

C. Evaporation of a Multi-component Aerosol

Equation (17) is valid for pure component aerosols; however, it has been established by (Saleh et al. 2012) that an “effective saturation concentration” and an “effective evaporation coefficient” can be used for multicomponent aerosols. Assuming an ideal mixture (or activity coefficient of unity), the effective α can be estimated as the evaporation rate weighted average α of the components and an effective saturation concentration of the mixture can be used to build the equilibration profile, where the effective saturation concentration is calculated as the mole weighted saturation concentration of the individual components of the aerosol particle. This approach is valid provided that the mole fraction of the individual components does not change significantly with time during measurements of particles concentrations throughout an experiment (Saleh et al. 2012). The absolute change in mole fraction has been found to be linearly correlated with the percentage change of mass concentration of the aerosol (Saleh et al. 2012). Hence, a convenient criterion for evaluating the validity of the approach is to check the ratio $\Delta C/C_0$ where ΔC is the maximum change in particle mass concentration throughout an experiment, and C_0 is the initial particle mass concentration. Simulations have revealed that a $\Delta C/C_0$ value less than 0.4 limits the deviation in the evaluated effective α from the actual pure components α to less than 25%.

D. The Phase Equilibration Method

Normalizing equation (17) by the effective saturation concentration $C_{\text{sat,eff}}$, replacing d_p by d_{cs} to account for polydispersity, we get the equation governing the change of the saturation ratio (C_g^*):

$$\frac{dC_g^*}{dt} = 2\pi N_{\text{tot}} d_{\text{cs,in}} \cdot D \cdot F_{\text{eff}} \cdot (K - C_g^*) \quad (19)$$

The definition of the saturation ratio as the ratio of the vapor concentration to the saturation concentration at the TD temperature makes its value an indicator on how far the aerosol sample is from restoring complete equilibrium where C_g^* will have a value of unity.

According to the Claiius-Clapeyron equation, the saturation concentration increases exponentially with increasing temperature as follows:

$$\left(\frac{C_{\text{sat1}} \cdot T_0}{C_{\text{sat0}} \cdot T_1} \right) = \exp \left(-\frac{\Delta H}{R} \left(\frac{1}{T_1} - \frac{1}{T_0} \right) \right) \quad (20)$$

Where ΔH is the enthalpy of vaporization of the aerosol in (J/Kg). Thus, when a positive step change in temperature is applied to an aerosol system, the saturation concentration becomes exponentially greater, and the saturation ratio drops well below unity and approaches 0; and hence, evaporation starts. The evolution of the saturation ratio from $C_g^* = 0$ to $C_g^* = 1$ constitutes the equilibration process.

Assuming the change in particle's diameter to be minimal, equation (19) can be treated as a first-order differential equation with a characteristic response time as shown:

$$\frac{dC_g^*}{dt} = \frac{1}{\tau} (K - C_g^*) \quad (21)$$

Where $\tau = \frac{1}{2\pi N_{\text{tot}} d_{\text{cs,in}} \cdot D \cdot F_{\text{eff}}}$ is called the "Equilibration Time Constant". Assuming a Kelvin factor of unity, an analytical solution for this equation would be:

$$C_g^* = 1 - e^{-\frac{t}{\tau}} \quad (22)$$

Physically speaking, “ τ ” represents the approximate characteristic time needed for an aerosol sample to reach a saturation ratio of $(1/e)$. So, in order for an aerosol sample to equilibrate completely within the TD dimensions, the residence time inside the TD should be larger than τ by “ e ” times, which renders τ a design guideline for the TD used in experiments. It should be noted that this claim is valid based on previous finding of (Saleh et al. 2011) where it has been proven that equilibration, as shown in equation (21), depends solely on the total aerosol length and mass transfer parameters D and F_{eff} .

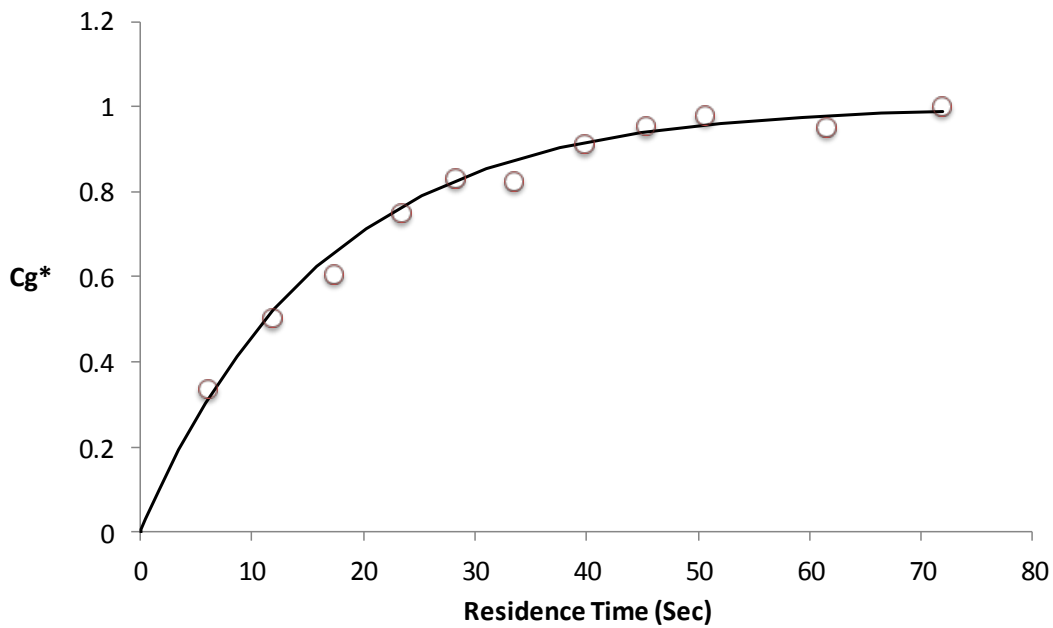


Figure 3: An Example of the Equilibration Profile

As noted in the first section, the only unknown parameter controlling an aerosol’s equilibration time (or τ) is the evaporation coefficient (α) that is embedded in the Sitarski-Nowakowski factor. This allows us to perform a single parameter fit to determine (α) once the profile of the saturation ratio C_g^* with time, otherwise called “The Equilibration Profile”, is

known. Hence, the equilibration method is based on estimating the gas phase concentration at different residence times in a TD. As the aerosol passes through the TD, particles start to evaporate, and the change in particles volume concentration will represent the change in gas phase concentration as illustrated earlier in equation (16). The saturation concentration, or volatility, is obtained from the last phase of the equilibration curve where the aerosol will have reached equilibrium as illustrated in Figure 3.

CHAPTER III

MATERIALS AND METHODS

In this work, polydisperse SOA is generated from engine exhaust using ultraviolet radiation. The SOA is introduced into a heated flow tube (“thermodenuder”, or TD) where it starts to evaporate until phase equilibrium is attained. The evolution of the particle volume concentration as a function of axial distance (and therefore residence time) from the tube inlet is monitored. The obtained data, consisting of particle volume concentration versus residence time, is then fitted to a theoretical model that describes the evolution of the particle volume concentration as an aerosol system approaches phase equilibrium. The theoretical model provides the evaporation coefficient that yields the least error between the experimental data and the prediction. In the below sections, the experimental setup and data analysis methods are presented. This chapter concludes with a presentation of key assumptions and their validity.

A. Experimental Setup

As shown in Figure 4, inside a mixing chamber, Secondary Organic Aerosol (SOA) was generated from volatile organic compounds (VOC’s) of gasoline engine exhaust using an ultraviolet lamp. After building up the setup that allowed us to obtain a feasible size distribution of the generated SOA, the aerosol was perturbed from equilibrium as it passed through a heated flow tube, or TD. By calculating the equilibration time constant (τ) based on the initial size distribution of particles, it was evident that equilibration is likely to occur within the residence time available in the TD. Using two Scanning Mobility Particle Sizers (SMPS), the evolution of particle volume concentration of the evaporating SOA was investigated by simultaneously

measuring the volume concentration upstream the TD and downstream the TD. Repeating this measurement at different residence times yielded a set of points that could be fitted to an evaporation kinetics model in order to determine the evaporation coefficient as will be described in the data analysis section. A total of 16 Experiments at different initial mass loadings were done, some of which has been ruled out for not following our validation criterion as will be explained in the Results section.

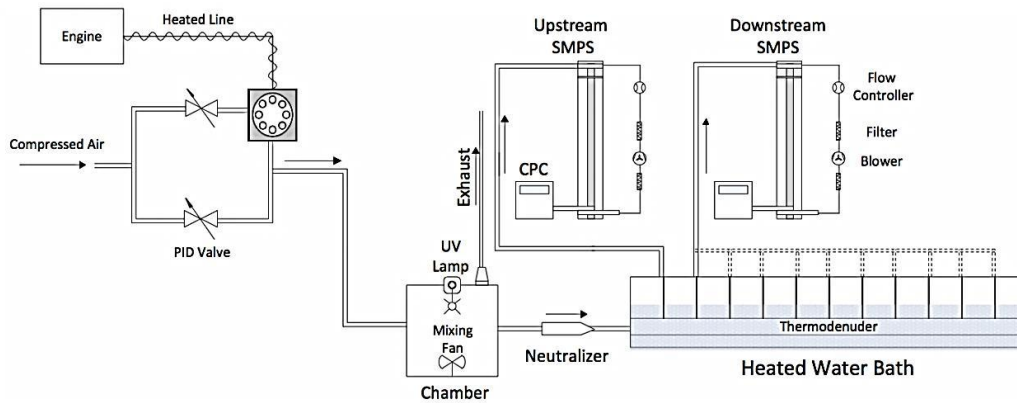


Figure 4: Experimental Setup for SOA Generation and Equilibration Profile Measurement

1. The Engine and the Exhaust System

The aerosol source was a typical single-cylinder gasoline engine (STEPHILL SHX1000) having 1 kVA capacity. The engine's rated normal speed is 5800 RPM at no load condition. The gasoline used is the 98 Octane type available in the local market. Lubricating oil used is SAE 10W-40 as recommended by the manufacturer. An engine-exhaust system has been installed where a sample of the exhaust was drawn. The part of the exhaust system carrying the aerosol to the Rotating Disk Diluter was heated to 170 °C to prevent condensation of gases.

2. The Rotating Disk Diluter

As its name applies, a Rotating Disk Diluter (MD19-3E, Matter Engineering) is mainly composed of an electrically heated block with a rotating disk having hemispherical cavities on its surface. The block-disk assembly is heated to prevent any vapors in exhaust to condense and form particles. As the sample will typically be cooled to ambient temperature as it is sent to a chamber, enough dilution is preferable to prevent condensation also at this stage. Air supplied to the diluter was filtered using a HEPA filter and passed through an Activated Carbon (AC) denuder to eliminate any volatile compounds. Air flow rate was controlled using a PID valve engaged to LabView interface. A built-in pump of the diluter withdrew a portion of the engine exhaust and both flows (Air and Exhaust) were directed to the rotating disk where they were mixed and the output was a diluted mixture that's sent through the Rotating Disk Diluter hose to the mixing chamber.

3. The PAM Chamber and the Ultra Violet (UV) Lamp

The chamber used in our setup was a 64 L box-shaped chamber with a mixing fan mounted on its ground to provide a good mixing for the aerosol before being sampled by the Scanning Mobility Particle Sizer (SMPS) system. A temperature and relative humidity (Rh) probe (Vaisala INTERCAP) was inserted into the chamber. The probe has an (Rh) range of 0 to 100%, and a temperature range of -40 °C to 60°C. On top of the chamber, a UV mercury lamp is mounted for launching SOA generation. The UV lamp light wavelength was 185 nm with a total length of 12 inches. This is basically the Potential Aerosol Mass approach, the concept of which was developed by (Kang et al. 2007). The term PAM is defined as the maximum aerosol mass that can be produced by oxidation of precursor gases (Kang et al. 2007). PAM measurements, according to (Kang et al. 2007), can be measured using a small, simple, flow through chamber

within a few minutes of exposure to high-energy source. So, a highly oxidizing environment is accomplished inside the flow through chamber where a major benefit of this approach is illustrated, which is the ability to complete experiments in hours instead of days as is the case in large environmental chambers (Kang et al. 2007).

4. The Thermo-denuder

The TD used in the experiments was a 1.5 m length stainless-steel tube having a 3.5 cm inner diameter with 14 equally spaced extraction ports mounted on its outer wall, in addition to the entrance and exit ports. A Teflon static mixer is placed at the entrance of the TD to ensure a plug flow of the aerosol at the beginning of the TD. The TD is placed inside a bath of water for the purpose of heating. A more uniform temperature distribution is achieved using this configuration than using a heating coil wrapped on the outer walls of the TD. The water bath is a 170x20x30 cm galvanized steel container. Water is heated using a circulatory water heating equipment (JULABO F33-ME) where temperature can be maintained constant throughout each run.

B. Procedure

Two Scanning Mobility Particle Sizers (SMPS) were used in our system. One SMPS was used to take samples upstream the TD, and another one was used to take samples downstream the TD at various ports. Each SMPS consisted of a Condensation Particle Counter (CPC) and a differential mobility analyzer (DMA) column. A CPC counts the number of particles in an aerosol sample by condensing alcohol on the particles so that they become large enough to scatter a laser beam of light and hence be counted. Maximum CPC count is 10,000 particles per cubic centimeter per size bin. In the DMA column is varied in such a manner as to separate particles and distribute them into size bins based on their electrical mobility. The measurable size

range of each SMPS spans a range of 10 nm to 560 nm at the standard operating conditions of 1 SLPM aerosol flow rate and 4 SLPM sheath flow rate SMPS scanning times were set to 60 sec in the increasing voltage mode.

Aerosol from engine exhaust is first drawn into the Rotating Disk Diluter (RDD) that operated at a Dilution Ratio (DR) of 5000:1. The diluter's block-disk assembly was heated to 120 °C to prevent condensation of gases from exhaust. Generated aerosol was then transported by means of the RDD built-in pump at a flow rate of 5 LPM into a stainless steel PAM chamber. The dilution air used for both the RDD and the chamber was always passed through a HEPA filter to ensure it is free of particles, and through an activated carbon (A.C.) denuder to make sure it is free of any volatile organic compounds. SOA was generated by exposing the received engine exhaust to UV radiation and the aerosol was diluted again with higher flow rates of zero air in order to decrease the residence time in the chamber so as to limit the growth of particles to the measurable size limits of our system. In order to achieve this, a trial-and-error method was followed by which the flow rate of dilution air through the chamber was varied until the size distribution of the aerosol leaving the chamber had a viable size distribution. By "viable" we mean steady and measureable in the SMPS size range window of 10-560 nm. A flow rate of 32 LPM was a suitable choice; therefore, a total of 37 LPM flow rate was the minimum flow rate through the PAM, which is equivalent to a total DR of about 32000:1 that simulates to a good extent typical atmospheric conditions (Robinson et al. 2007; Ning and Sioutas 2010). Higher flow rates through the PAM would give higher DR; and hence, lower mass concentrations of SOA.

The aerosol was then sent to the TD that was maintained at a constant temperature (see Experimental Conditions section below) in order to perturb the aerosol from equilibrium to be

able to observe its evaporation kinetics. To avoid any potential effect (e.g. deposition) of the entrance port being different in geometry than other sampling ports, the aerosol was first sent to the TD through the entrance port, and a stainless steel two-way splitter was installed on the first port that is identical to other sampling ports. The splitter was used to allow the two SMPS's take samples at the same port in order to inter-calibrate the system. Inter-calibration was done based on the volume concentration in order to account for any difference between the two instruments when computing changes in volume concentrations DS the TD. The same applied for the number concentration where the inter-calibration was done base on the number concentrations at the same port. Downstream sampling started at the second port and was repeated at the various ports. The flow rate of each of the upstream and downstream SMPSs is 1 LPM allowing for a maximum residence time of almost 90 sec inside the TD.

C. Experimental Conditions

In all experiments, engine operated at no load condition and the carbon monoxide (CO) concentration was measured and was typically 8% to 9%. The exhaust line was heated to 170°C, the diluter operated at a DR of 5000:1 with a flow rate of 5 LPM, and the diluter block-disk assembly was heated to 120°C. The ratio of the sheath to aerosol flow rate in the SMPS was 4:1. Prior to an experiment, the aerosol was allowed to pass through the TD for half an hour to ensure wall passivation. A total of 5 particle size scans was made at each port. A limited number of experiments utilized TD temperatures of 50°C and 60°C. It was found, however, that the 40°C condition provided sufficient deflection in particle volume concentration. For this reason, remaining measurements were done at this temperature since it is most representative of ambient conditions. The aerosol flow in the TD was maintained at 1 LPM. Out of a total of 16 experiments 8 valid data sets were obtained. Data sets were considered valid when the upstream

particle mass concentration did not drift more than 10% of the mean for the duration of the experiment, and when the ratio $\Delta C/C_0$ was less than 0.4 at the TD exit.

D. Data Analysis

As evaporation of particles evolve, two pathways are possible for the vapors escaping particles: diffusion to the TD walls, and to the bulk (gas) of the aerosol. TD walls were considered as a zero flux boundary as they have been passivated with the aerosol prior to equilibration experiments. Applying mass conservation principle, this allows us to write the following expression:

$$\Delta m_p = -\Delta C_g \quad (23)$$

Furthermore, assuming a constant density of SOA of 1 g/cc (Odum et al. 1997), we can write:

$$\Delta m_p(t) = \rho \Delta V_p(t) \quad (24)$$

Thus, we get the relation that relates the change in gas phase concentration to the change in particles volume concentration:

$$\Delta C_g(t) = \rho \Delta V_p(t) \quad (25)$$

Going back to the equilibration profile equation (19), we need to have an expression for the saturation ratio, $C_g^*(t)$. By definition, we have:

$$C_g^*(t) = \frac{C_g(t)}{C_{sat}(T_1)} \quad (26)$$

$$\Delta C_g(t) = C_g(t) - C_{sat}(T_0) \quad (27)$$

$$\Delta C_{g, equilibrium}(T_1) = C_{sat}(T_1) - C_{sat}(T_0) \quad (28)$$

For reasonable values of the enthalpy of vaporization of ambient semi-volatile organics ($\Delta H \approx 50 - 100$ kJ/mol) (Saleh et al. 2009), the ratio of saturation concentration (C_{sat}) at

ambient temperature $T_0 = 24 \text{ }^\circ\text{C} (\pm 1^\circ\text{C})$ to the saturation concentration (C_{sat}) at the temperature of the TD ($T_1 = 40 \text{ }^\circ\text{C}$) is of the order of 1%, which allows us to write:

$$C_g^*(t) \approx \frac{\Delta C_g(t)}{\Delta C_{g, equilibrium}(T_1)} \quad (29)$$

Substituting Eq 25 in Eq 29, we get the relation:

$$C_g^*(t) = \frac{\Delta V_p(t)}{\Delta V_{p, equilibrium}} \quad (30)$$

Eq 30 implies that by measuring $\Delta V_p(t)$ and $\Delta V_{p, equilibrium}$ we can calculate the equilibration profile, $C_g^*(t)$, which is needed as input to equation (19) (recalled below):

$$\frac{dC_g^*}{dt} = 2\pi N_{tot} d_{cs, in} \cdot D \cdot F_{eff} \cdot (K - C_g^*) \quad (31)$$

Other required inputs are the diffusivity (D) of the gas, and the Sitarski-Nowakowski (F) interpolation factor. Gas diffusivity (D) is estimated using Chapman-Enskog formula (Reid et al. 1987) to be $5e-6 \text{ m}^2/\text{sec}$, while F is defined as:

$$F = \frac{b(1+a \cdot Kn)}{b+c \cdot Kn+d \cdot Kn^2} \quad (32)$$

Where the Knudsen number (Kn) and the parameters a, b, c, and d are defined in Table 1 as follows:

Kn	a	b	c	d
$\frac{2\lambda}{d}$	$\frac{3\beta(1+z)^2}{4(3+5z)}$	$\frac{4(9+10z)}{15\pi(1+z)^2}$	$\frac{\beta(1+2z)}{\pi(3+5z)} + \frac{1}{2\beta}$	$\frac{9(1+z)^2}{8(3+5z)}$

Table 1: Parameters of Equation 32

Wherein the expression of the MFP of air (λ) is that used by (Sitarski and Nowakowski 1979) in their definition of the Knudsen number and it is defined along with β and z in Table 2 as follows:

λ	z	β
$\frac{32}{3\pi(1+z)} * \frac{D}{\bar{c}_A}$	$\frac{M_A}{M_B}$	$\frac{\alpha}{2-\alpha}$

Table 2: Parameters of Table 1

Where M_A is the molecular weight of the evaporating aerosol and M_B is the molecular weight of air, α is the evaporation coefficient, and \bar{c}_A is the mean molecular speed corresponding to a Maxwell-Boltzmann distribution of velocity for the desorbing molecules and it is given as:

$$\bar{c}_A = \sqrt{\frac{8kT}{\pi M_B}} \quad (33)$$

In which k is the Boltzmann Constant, and T is temperature in (K).

As mentioned in the Theory section, other interpolation factors are available in the literature; however, none of these factors accounts for the molecular weight ratio (z) except for the Sitarski-Nowakowski factor that is valid for (z) values above unity unlike other factors (Li and Davis 1996). In our study, the molecular weight of SOA constituents on average is higher than that of air. With M_B of 0.028 kg/mol and M_A of 0.15 kg/mol, we get $z=5.3$. Thus the system of interest will consist of relatively heavy molecules suspended in lighter background gas molecules, which is the condition accounted for in Eq 32 (Li and Davis 1996).

Matlab ODE45 solver is used to solve Eq 19. The solver takes initial saturation concentration, temperature, and condensation sink diameter as initial conditions and returns the equilibration profile $C_g^*(t)$. This solution is repeated over a range of values of α spanning between 0 and 1 with a step of 0.01. An optimization loop chooses the theoretical time steps that coincides with the experimental time steps and calculates the mean square error of the corresponding experimental and theoretical C_g^* values. The value of α that gives the least error is outputted as the effective α for the data in question.

E. Assumptions Validation

Assumptions made in our analysis were negligible particle deposition to the TD walls and a kelvin factor of unity. In this section, we investigate the validity of these two assumptions.

Volume concentration of particles was simultaneously measured upstream of the TD and downstream of it. Eventually, a dataset of particle volume concentration differences (ΔV_p) versus time was obtained. Particle volume concentration can decrease due to evaporation, or due to deposition, or both. As the particles number concentration downstream of the TD were similar to that upstream of the TD, deposition was considered to be negligible. The average ratio of upstream to downstream number concentrations for the valid experiments was 0.94 (± 0.02). Therefore, a decrease in particles volume concentration was taken as evidence on particles evaporation.

To investigate the effect of the Kelvin factor (K) on our results, we did simulations assuming a value for the surface tension (σ). As (K) is inversely proportional to diameter, the simulation was done on the data set having the smallest initial condensation sink diameter. In Figure 5, set (1) is the set of ΔV values generated by incorporating the Kelvin effect into the equilibration profile equation by setting (σ) to 0.17 N/m (or $K=1.638$). Setting (σ) to 0 N/m (or $K=1$), gives set (2). Sets (1) and (2) are in good agreement up to an Equilibration parameter (t/τ) of 3, after which set (2) starts to deviate away from set (1). This is due to the difference in concentration at equilibrium between the wall having (C_{sat}) and the particles being at ($K C_{sat}$), which will drive the particles to evaporate until they all partition into the gas phase. However, sets (1) and (2) yield the same evaporation coefficient when fitted to the experimental data, which makes it reasonable to assume a Kelvin factor of unity while investigating the evaporation coefficient.

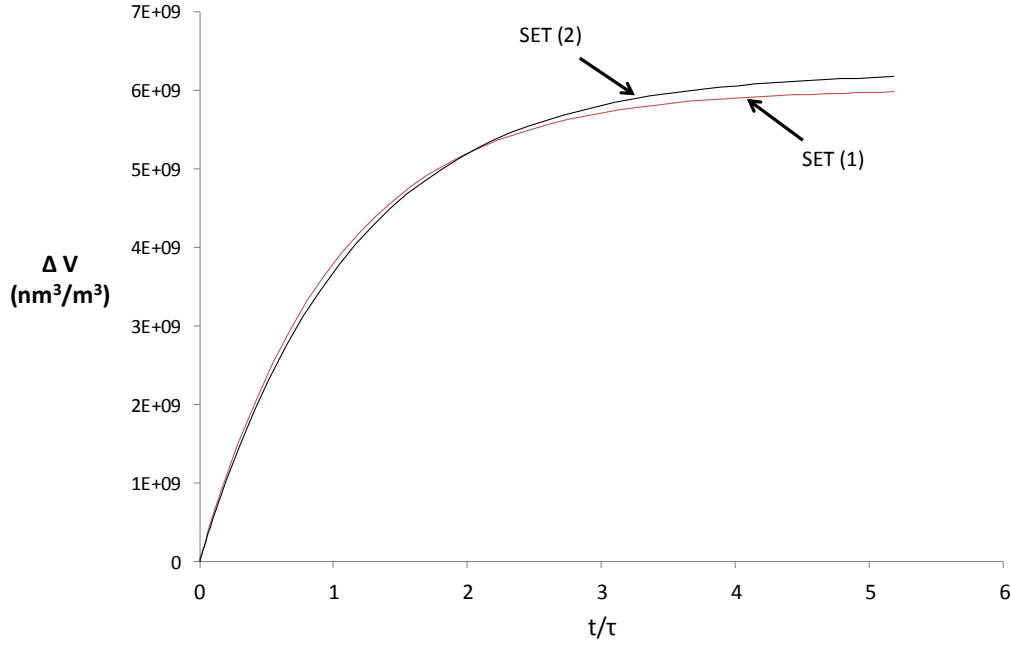


Figure 5: Simulations illustrating the effect of incorporating the Kelvin factor into the data analysis. Surface tension value used was 0.17 N/m resulting in a kelvin factor of 1.68 when applied on the dataset of the minimum condensation sink diameter.

F. Uncertainty Analysis

To assess uncertainty in the obtained α , a Monte Carlo approach was used where a 100 simulations were performed to perturb the experimental values of C_g^* to a value equal to $\overline{C_g^*} + \sigma\phi$ where $\overline{C_g^*}$ is the mean value of measured C_g^* at each port, σ is the standard deviation of the measurements, and ϕ is a random variable drawn from a standard normal distribution (mean of 0 and standard deviation of 1). Results of these simulations are used to calculate the uncertainty in the obtained evaporation coefficients.

CHAPTER IV RESULTS

A. SOA Generation

To demonstrate that we are generating SOA particles from precursors found in gasoline engine exhaust, a set of different experimental conditions was tested. As illustrated in Figure 6, concentration downstream of the PAM chamber was measured while keeping UV radiation off (condition A). Then, UV radiation was turned ON and no generation of particles was recorded (condition B). Upon allowing engine exhaust that was diluted with humid air to enter the chamber, a rapid increase in concentration is recorded indicating generating of SOA particles (condition C). Replacing humid air with filtered, low humidity air, SOA concentration dropped to a lower value, which is an observation consistent with the SOA generation phenomena where the more available the water vapor, the more available are the OH radicals (condition D). Finally, turning off the UV radiation while maintaining the engine exhaust and dilution air flows constant (Condition E) returns the particle concentration in chamber to its initial near-zero value.

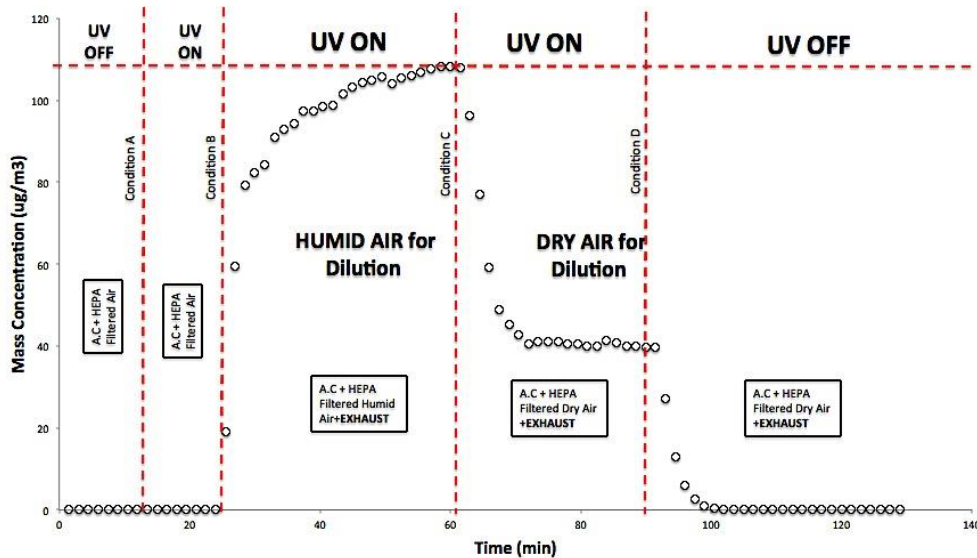


Figure 6: Evolution of SOA Mass Concentration inside the PAM Chamber (typical results)

B. Particle Size Distribution

In Table 3, initial conditions downstream of the chamber for experiments conducted at 40 °C that followed our validation criterion are presented. Initial mass loadings for all experiments ranged between $18\mu\text{g}/\text{m}^3$ and $40\mu\text{g}/\text{m}^3$, and aerosol flow rate through the TD was 1 LPM (Re=30). The temperature and relative humidity inside the chamber for each experiment are shown in Table 4 along with the initial mass loadings.

Experiment	Initial	Initial	Mode Diameter		Geometric		Maximum
	Number	Volume	(nm)		Standard		Change in
	Concentration (particles/m ³)	Loading (nm ³ /m ³)	US	DS	US	DS	Volume (nm ³ /m ³)
1	7.65E+10	2.74E+10	142(±9)	136(±5)	1.57	1.59	6.02E+09
2	6.09E+10	5.86E+10	175(±10)	165(±9)	1.57	1.59	7.03E+09
3	4.86E+10	1.31E+10	148(±12)	139(±6)	1.57	1.59	4.32E+09
4	5.47E+10	1.83E+10	142(±3)	132(±9)	1.57	1.58	4.03E+09
5	5.31E+10	2.04E+10	147(±9)	136(±7)	1.57	1.58	4.28E+09

Table 3: Size Distribution Characteristics - US = Upstream TD (Measurement taken US the First Port) - DS = Downstream TD (Measurement Taken DS the Last Port)

Experiment	Chamber Temperature (°C)	Chamber Relative Humidity (%)	Mass Loading ($\mu\text{g}/\text{m}^3$)
1	22	12	26
2	25	14	34
3	25	13	19
4	24	12	18
5	25	14	19

Table 4: Chamber Temperature, Rh, and Mass Loading for Each Experiment

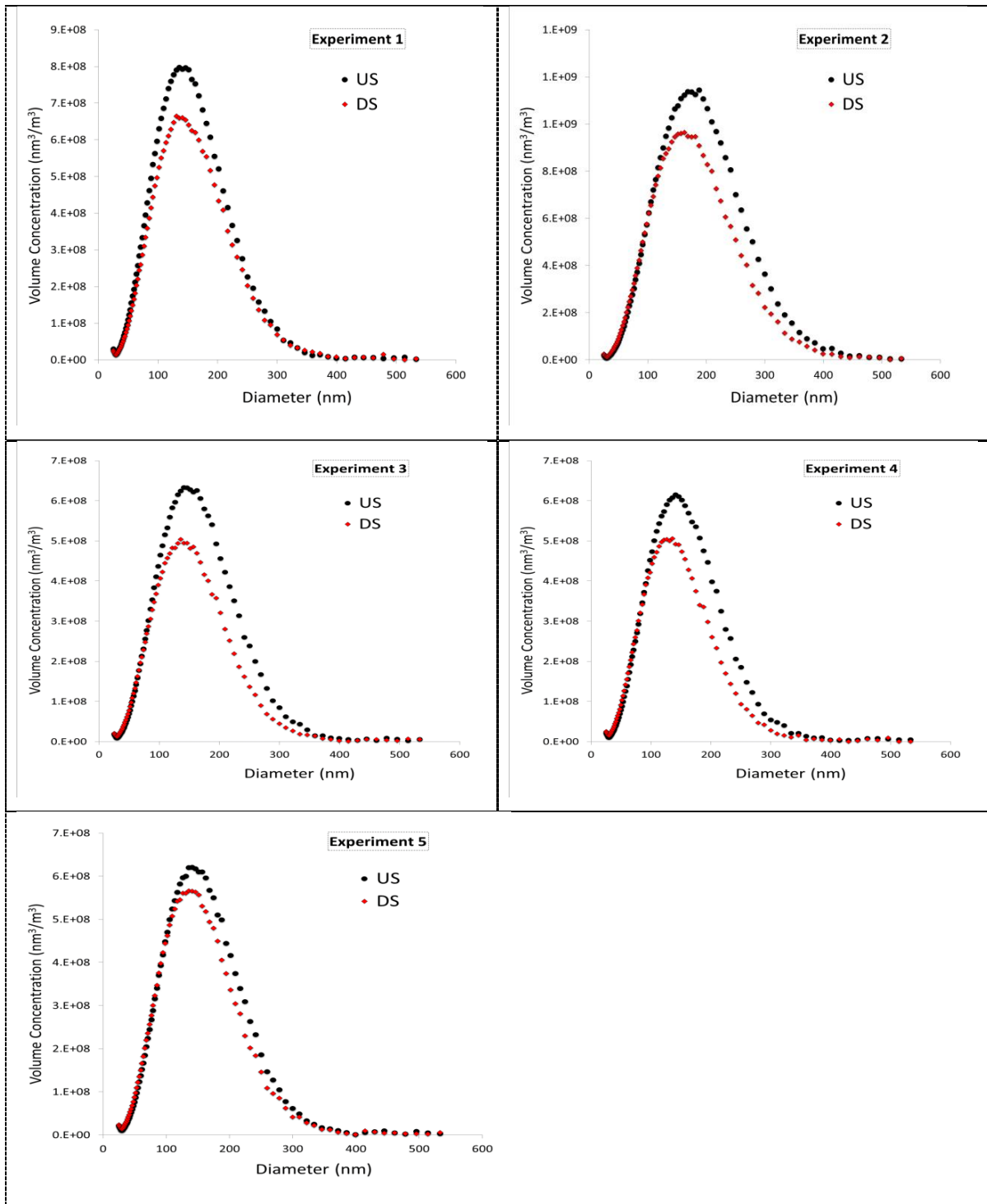


Figure 7: US and DS Size Distributions for Experiments 1 Through 5

Figure 7 shows the size distributions for experiments 1 through 5. All distributions had a typical lognormal distribution. Upper and lower limit sizes are within the SMPS's measurement range. The DS distribution always had its peak shifted towards smaller diameter values compared to the US distribution, which is consistent with evaporation.

C. Equilibration Profile

Experiments 1 through 5 exhibited good agreement with the kinetics model. Shown in Figure 8 are the profiles of predicted change in aerosol volume concentration for 3 of the experiments plotted in terms of residence time in TD. As the initial mass loadings were different among experiments, the equilibrium values of ΔV_p changed. To prove that our aerosol system had a similar behavior in all experiments and that our approach gives the same evaporation coefficient even if the initial mass loadings were different, data is normalized by the equilibrium value of ΔV_p , which gives us the saturation ratio $C_g^*(t)$ as demonstrated in the data analysis section. Equilibrium value of ΔV_p is taken as the average of ΔV_p values at the ports where the change in $\Delta V_p(t)$ stopped, and residence times are normalized by the equilibration time constant (τ). As shown in Figure 9, all points collapse into the universal phase equilibration curve defined by equation (19).

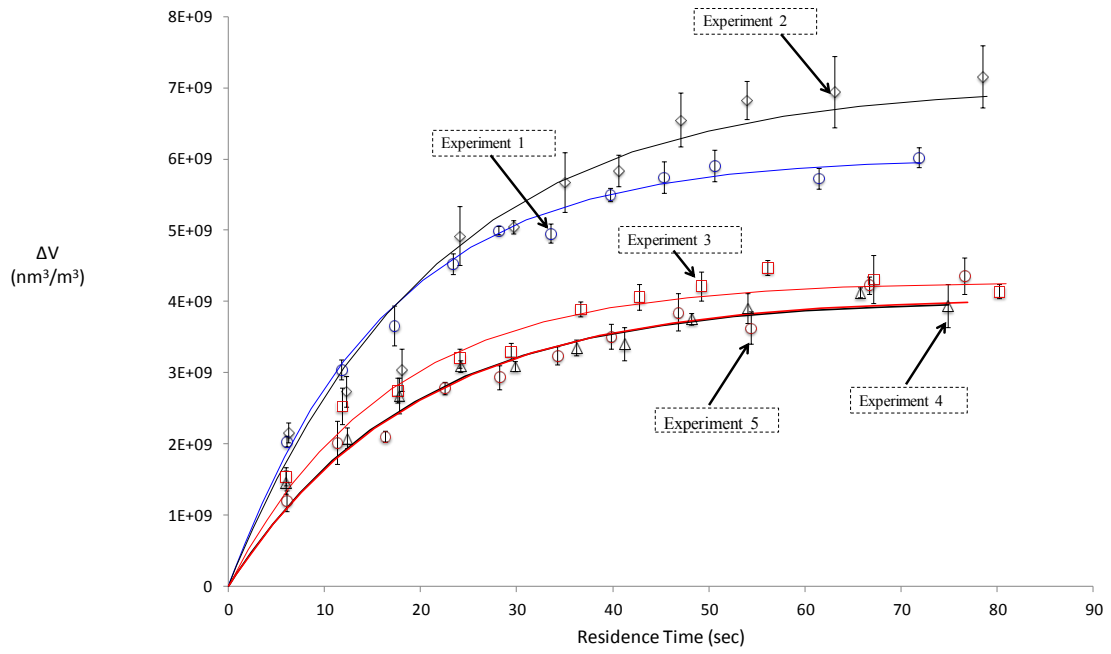


Figure 8: Dimensional Equilibration Profiles for 5 Experiments Having Different Initial Loadings

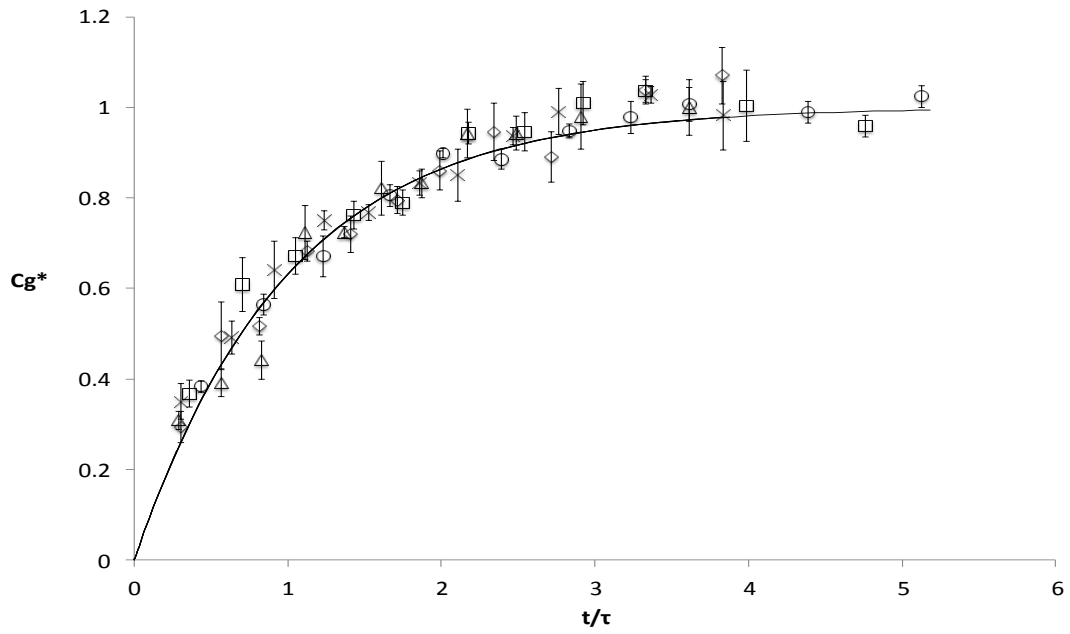


Figure 9: Non-dimensional Equilibration Profiles for the 5 Experiments

D. Effective Evaporation Coefficient

Table 5 summarizes the obtained effective evaporation coefficients and the effective saturation concentrations for the five experiments. Presented also are the key parameters of the equilibration process along with the goodness of the fit for each experiment.

Experiment	τ (sec)	R^2	$\Delta C/C_0$	α_{eff}	$C_{\text{sat,eff}}(25^\circ\text{C})$ [$\mu\text{g}/\text{m}^3$]
1	13	0.98	0.22	0.87(± 0.17)	2.4
2	16	0.94	0.12	0.89(± 0.19)	1.7
3	21	0.96	0.33	0.82(± 0.24)	2.8
4	19	0.97	0.22	0.82(± 0.22)	1.6
5	19	0.95	0.21	0.84(± 0.19)	1.6

Table 5: Critical Parameters and Obtained Evaporation Coefficients where the \pm values are standard deviation of the values resulting from the uncertainty analysis

The condition $\Delta C/C_0 < 0.4$ was met for all experiments. All obtained apparent evaporation coefficients are approaching unity, and characteristic equilibration times ranged from 13 to 21 sec. An enthalpy of vaporization of 50 kJ/mol was assumed to get $C_{\text{sat,eff}}(25^\circ\text{C})$ from $C_{\text{sat,eff}}(T_{\text{TD}})$.

CHAPTER V

DISCUSSION AND ANALYSIS

While several recent investigations in the atmospheric aerosols literature suggest that SOA cannot equilibrate within atmospheric timescales, our results indicate that anthropogenic SOA are well characterized by absorptive partitioning theory and are not intrinsically mass transfer inhibited. This study indicates that atmospheric SOA will equilibrate within short timescales, an assumption that is widely employed in most current air quality models. In this section, we discuss the findings of this study and compare them with previously published data. We place our reported evaporation coefficient and volatility values in the context of air quality modeling and clarify their atmospheric implications.

A. SOA Gas-particle Particle Partitioning

Applied to OA, conventional absorptive partitioning theory assumes that aerosol particles are internally well-mixed and that individual species are capable of evaporating from the particle surface at a rate proportional to their mole fractions and vapor pressures (Pankow 1994). The fact that SOA evaporation kinetics in this study are well described by this model suggests that SOA evaporation follows partitioning theory. Our results demonstrate that SOA of anthropogenic origin responds to temperature change by evaporation and equilibrates within the residence times available in our thermodenuder (order of a minute). Based on the condensation sink diameter of the generated particles and on the value of α reported, extrapolating the equilibration timescales to atmospherically relevant SOA concentrations ($<5 \mu\text{g}/\text{m}^3$) yields values in the order of minutes, which underpins the assumption of equilibrium currently applied in models. The significance of the technique used in this study to investigate gas-particle partitioning (Saleh et al. 2011) is best

shown in Figure 9 where equilibration profiles for partitioning of SOA samples having different initial mass loadings collapse into a single curve.

B. Effect of Evaporation Coefficient

A widely used representation of SVOA volatility is the so-called “Volatility Basis Set, or VBS” introduced by (Donahue et al. 2006) wherein the OA mass is sorted into bins of logarithmically spaced volatilities, or effective saturation concentrations. In this study, no assumptions were made on the volatility of the evaporating species. It is of interest, hence, to evaluate how the measured volatility compares with values reported by other investigators. (Faulhaber et al. 2009) reported on the volatility of freshly lab-generated anthropogenic SOA using a calibration curve for some standard compounds and assuming α values between 0.3 and 1 and enthalpy of vaporization between 129 and 174 kJ/mol. Using the VBS representation (Donahue et al. 2006), they reported a set of $C_{\text{sat}}(25^\circ\text{C})$ spanning the range 10^{-4} to 10^2 $\mu\text{g}/\text{m}^3$ with the majority of the compounds being in the 10^{-3} to 10 $\mu\text{g}/\text{m}^3$ range. Volatility of SOA in our system falls within this range as has been demonstrated in the results section. (Cappa and Jimenez 2010) found that ambient OA had much lower volatilities. For α values between 0.1 and unity and an enthalpy of vaporization of 50 kJ/mol, they reported $C_{\text{sat}}(25^\circ\text{C})$ between 10^{-6} and 10^{-2} $\mu\text{g}/\text{m}^3$. It should be noted, however, that ambient OA that (Cappa and Jimenez 2010) investigated had undergone aging in the atmosphere, unlike our study and that of (Faulhaber et al. 2009). Using a thermodenuder combined with Aerosol Mass Spectrometry (AMS) and an SMPS system, (Lee et al. 2010) measurements of ambient secondary organic aerosol volatility distribution was found to lie in the range of 0.01-1 $\mu\text{g}/\text{m}^3$ for an evaporation coefficient of 1 and enthalpy of vaporization of 80 kJ/mol. Whether the

assumptions on the enthalpy of vaporization made in these studies are consistent with those estimated in our study and implications of this will be investigated in the next section.

Finally, it should also be noted that the combination of the volatility and the evaporation coefficient that gave a good fit with our experimental data is unique. This is explained by the following theoretical experiment. If we force α to take a value order 0.01 or less, there is no value of $\Delta V_{equilibrium}$ that can produce a reasonable fit to the experimental data. Two examples corresponding to α values of 10^{-4} and 0.01 are shown in Figure 10 and 11 below. This result supports the notion that the effective evaporation coefficients observed in this study are well constrained to the 0.1-1 decade, in contrast to the aforementioned studies.

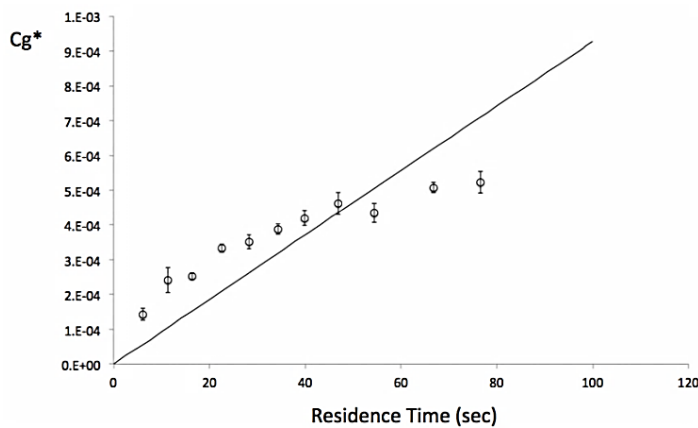


Figure 10: Best Possible Fit for Equilibration Process based on $\alpha=10^{-4}$

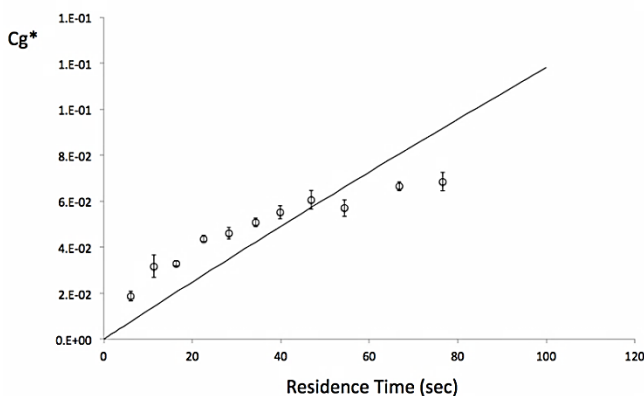


Figure 11: Best Possible Fit for Equilibration Process based on $\alpha=0.01$

C. Effect of Temperature

As mentioned earlier, other experiments were conducted at temperatures higher than 40 °C at the beginning of our investigation. While the obtained evaporation coefficients did not vary significantly for experiments of different temperatures, the maximum change in ΔV (i.e. $\Delta V_{\text{equilibrium}}$) did change. Figure 12 shows that $\Delta V_{\text{equilibrium}}$ increased with increasing temperature, which is also consistent with evaporation.

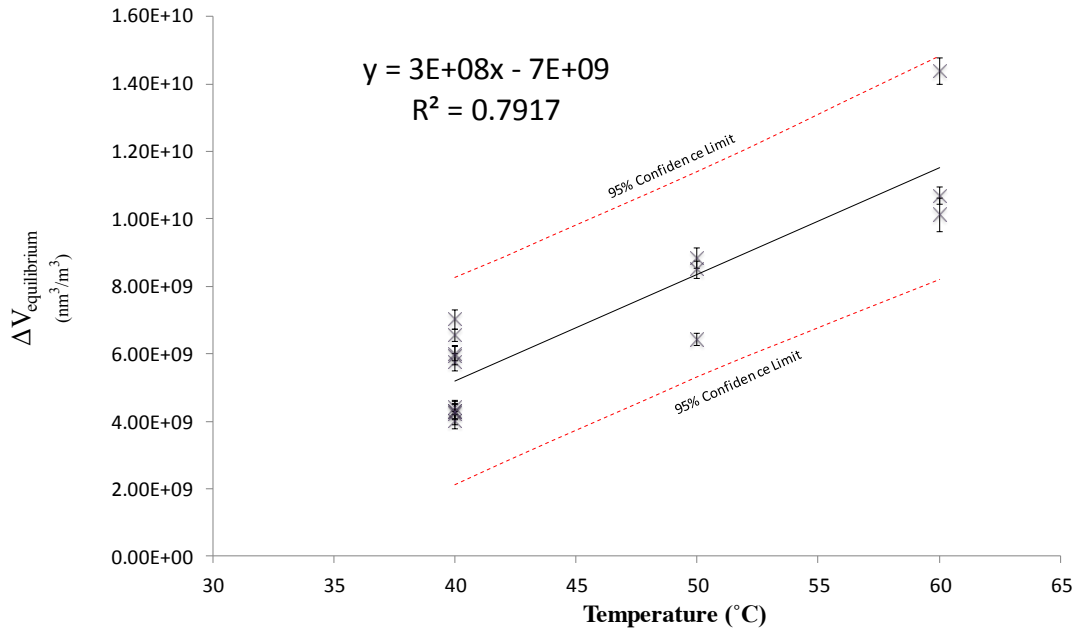


Figure 12: Temperature Effect on Maximum Change in Particles Volume through the TD

Using the Clausius-clapeyron equation, enthalpy of vaporization can be estimated as:

$$\Delta H = \frac{-R \ln \left(\frac{T_2 \Delta V_{\text{equilibrium},2}}{T_1 \Delta V_{\text{equilibrium},1}} \right)}{\frac{1}{T_2} - \frac{1}{T_1}}$$

Using the fitted equation, the average values of $\Delta V_{equilibrium,1}$ and $\Delta V_{equilibrium,2}$ are determined for $T_1 = 40\text{ }^\circ\text{C}$ and $T_2 = 60\text{ }^\circ\text{C}$, respectively. This gives a value of 36 kJ/mol. Similarly, the values of $\Delta V_{equilibrium}$ at the 90% confidence limits on the fit are determined, which gives ΔH values in the range of 28 kJ/mol to 61 kJ/mol. The value of 50 kJ/mol used to calculate the effective saturation concentration at 25 °C falls in this range. Using higher values of ΔH such as 100 kJ/mol, which is typical for atmospheric aerosols (Epstein et al. 2009), the values of our reported volatilities would shift 1 order of magnitude towards lower volatility bins. This, however, keeps SOA volatility measured in this study in the range of values reported in the literature.

D. Limitations

This study tackled evaporation kinetics of freshly generated SOA that may not mimic the aged atmospheric SOA. The implications of this issue have been discussed in section (V). Initial mass loadings are also higher than that in the atmosphere, which might have biased our results towards more volatile compounds. However, this does not change our conclusions on the mass transfer part of the problem as the method we use does not depend on volatility of the investigated aerosols. A major difficulty faced in the experimental setup was obtaining a steady aerosol concentration in the PAM chamber.

E. Recommendations

Future enhancement of the setup used in this study to generate SOA is recommended in order to achieve better stability of the generation process. Mixing of gasoline engine emissions with diesel engine emissions would provide a better simulation of the atmosphere. Concentration of hydroxyl radicals in the chamber could be estimated through measuring decay of VOC's

concentrations. This would provide us with valuable information on how close we are to atmospheric levels and timescales of OH exposure. Experiments at lower temperatures are also of interest as well as allowing for aging of the generated SOA and investigating their evaporation kinetics.

CHAPTER VI

CONCLUSION

Stable SOA production and measurable size distributions have been attained using the PAM technique. The phase equilibration method has been used to determine the effective evaporation coefficient of SOA generated from real engine gasoline exhaust. Experimental data showed excellent agreement with a kinetics model used to describe the equilibration process in a thermodenuder. An effective evaporation coefficient approaching unity has been reported. This finding is of significant importance for aerosol volatility studies and for prediction of SOA concentrations in the atmosphere. Another outcome for this work is volatility of freshly lab-generated SOA that has been found to lie within the range of volatilities reported in literature for lab-generated SOA. Behavior of SOA particles in the atmosphere is not likely to show extreme mass transfer inhibition, and equilibration of such particles is expected to occur within atmospheric timescales.

BIBLIOGRAPHY

- Cappa, C., and Jimenez, J. (2010). "Quantitative estimates of the volatility of ambient organic aerosol." *Atmospheric Chemistry and Physics*, 10(12), 5409-5424.
- Cappa, C. D., and Wilson, K. (2011). "Evolution of organic aerosol mass spectra upon heating: implications for OA phase and partitioning behavior." *Atmospheric Chemistry and Physics*, 11(5), 1895-1911.
- Chang, J., and Hanna, S. (2004). "Air quality model performance evaluation." *Meteorology and Atmospheric Physics*, 87(1-3), 167-196.
- Chow, J. C., Watson, J. G., Fujita, E. M., Lu, Z., Lawson, D. R., and Ashbaugh, L. L. (1994). "Temporal and spatial variations of PM_{2.5} and PM₁₀ aerosol in the Southern California air quality study." *Atmos. Environ.*, 28(12), 2061-2080.
- Davis, E. J., and Schweiger, G. (2002). *The airborne microparticle: its physics, chemistry, optics, and transport phenomena.* Springer, .
- Donahue, N., Robinson, A., Stanier, C., and Pandis, S. (2006). "Coupled partitioning, dilution, and chemical aging of semivolatile organics." *Environ.Sci.Technol.*, 40(8), 2635-2643.
- Epstein, S. A., Riipinen, I., and Donahue, N. M. (2009). "A semiempirical correlation between enthalpy of vaporization and saturation concentration for organic aerosol." *Environ.Sci.Technol.*, 44(2), 743-748.
- Faulhaber, A., Thomas, B., Jimenez, J., Jayne, J., Worsnop, D., and Ziemann, P. (2009). "Characterization of a thermodenuder-particle beam mass spectrometer system for the study of organic aerosol volatility and composition." *Atmospheric Measurement Techniques*, 2(1), 15-31.
- Gordon, T., Presto, A., May, A., Nguyen, N., Lipsky, E., Donahue, N., Gutierrez, A., Zhang, M., Maddox, C., and Rieger, P. (2013). "Secondary organic aerosol formation exceeds primary particulate matter emissions for light-duty gasoline vehicles." *Atmospheric Chemistry and Physics Discussions*, 13(9), 23173-23216.
- Hall IV, W. A., and Johnston, M. V. (2011). "Oligomer content of α -pinene secondary organic aerosol." *Aerosol Science and Technology*, 45(1), 37-45.
- Hallquist, M., Wenger, J., Baltensperger, U., Rudich, Y., Simpson, D., Claeys, M., Dommen, J., Donahue, N., George, C., and Goldstein, A. (2009). "The formation, properties and impact of secondary organic aerosol: current and emerging issues." *Atmospheric Chemistry and Physics*, 9(14), 5155-5236.
- Haywood, J., and Boucher, O. (2000). "Estimates of the direct and indirect radiative forcing due to tropospheric aerosols: A review." *Rev.Geophys.*, 38(4), 513-543.

Henze, D., Seinfeld, J., Ng, N., Kroll, J., Fu, T., Jacob, D., and Heald, C. (2008). "Global modeling of secondary organic aerosol formation from aromatic hydrocarbons: High-vs. low-yield pathways." *Atmospheric Chemistry and Physics*, 8(9), 2405-2420.

Hinds, W. C. (2012). *Aerosol technology: properties, behavior, and measurement of airborne particles*. John Wiley & Sons, .

Kanakidou, M., Seinfeld, J., Pandis, S., Barnes, I., Dentener, F., Facchini, M., Dingenen, R. V., Ervens, B., Nenes, A., and Nielsen, C. (2005). "Organic aerosol and global climate modelling: a review." *Atmospheric Chemistry and Physics*, 5(4), 1053-1123.

Kang, E., Root, M., Toohey, D., and Brune, W. (2007). "Introducing the concept of potential aerosol mass (PAM)." *Atmospheric Chemistry and Physics*, 7(22), 5727-5744.

Lee, B., Kostenidou, E., Hildebrandt, L., Riipinen, I., Engelhart, G., Mohr, C., DeCarlo, P., Mihalopoulos, N., Prevot, A., and Baltensperger, U. (2010). "Measurement of the ambient organic aerosol volatility distribution: application during the Finokalia Aerosol Measurement Experiment (FAME-2008)." *Atmospheric Chemistry and Physics*, 10(24), 12149-12160.

Lehtinen, K. E., Korhonen, H., Maso, M., and Kulmala, M. (2003). "On the concept of condensation sink diameter." *Boreal Environ.Res.*, 8(4), 405-412.

Li, W., and Davis, E. J. (1996). "Aerosol evaporation in the transition regime." *Aerosol Science and Technology*, 25(1), 11-21.

Maxwell, J. C. (1890). *The Scientific Papers of James Clerk Maxwell... J. Hermann, .*

Moore, W. (1962). "Physical Chemistry. 3-rd ed." .

Ning, Z., and Sioutas, C. (2010). "Atmospheric processes influencing aerosols generated by combustion and the inference of their impact on public exposure: a review." *Aerosol and Air Quality Research*, 10(1), 43-58.

Odum, J. R., Jungkamp, T., Griffin, R., Flagan, R. C., and Seinfeld, J. H. (1997). "The atmospheric aerosol-forming potential of whole gasoline vapor." *Science*, 276(5309), 96-99.

Pankow, J. F. (1994). "An absorption model of gas/particle partitioning of organic compounds in the atmosphere." *Atmos. Environ.*, 28(2), 185-188.

Pankow, J. F. (1994). "An absorption model of the gas/aerosol partitioning involved in the formation of secondary organic aerosol." *Atmos. Environ.*, 28(2), 189-193.

Pankow, J. F., and Barsanti, K. C. (2009). "The carbon number-polarity grid: A means to manage the complexity of the mix of organic compounds when modeling atmospheric organic particulate matter." *Atmos. Environ.*, 43(17), 2829-2835.

Pathak, R., Presto, A., Lane, T., Stanier, C., Donahue, N., and Pandis, S. (2007). "Ozonolysis of α -pinene: parameterization of secondary organic aerosol mass fraction." *Atmospheric Chemistry and Physics*, 7(14), 3811-3821.

Perraud, V., Bruns, E. A., Ezell, M. J., Johnson, S. N., Yu, Y., Alexander, M. L., Zelenyuk, A., Imre, D., Chang, W. L., and Dabdub, D. (2012). "Nonequilibrium atmospheric secondary organic aerosol formation and growth." *Proceedings of the National Academy of Sciences*, 109(8), 2836-2841.

Pöschl, U. (2005). "Atmospheric aerosols: Composition, transformation, climate and health effects." *Angewandte Chemie International Edition*, 44(46), 7520-7540.

Pun, B. K., Griffin, R. J., Seigneur, C., and Seinfeld, J. H. (2002). "Secondary organic aerosol 2. Thermodynamic model for gas/particle partitioning of molecular constituents." *Journal of Geophysical Research*, 107(D17), 4333.

Rader, D., McMurry, P., and Smith, S. (1987). "Evaporation rates of monodisperse organic aerosols in the 0.02-to 0.2- μ m-diameter range." *Aerosol Science and Technology*, 6(3), 247-260.

Reid, R. C., Prausnitz, J. M., and Poling, B. E. (1987). "The properties of gases and liquids." .

Robinson, A. L., Donahue, N. M., Shrivastava, M. K., Weitkamp, E. A., Sage, A. M., Grieshop, A. P., Lane, T. E., Pierce, J. R., and Pandis, S. N. (2007). "Rethinking organic aerosols: Semivolatile emissions and photochemical aging." *Science*, 315(5816), 1259-1262.

Saleh, R., Shihadeh, A., and Khlystov, A. (2011). "On transport phenomena and equilibration time scales in thermodenuders." *Atmospheric Measurement Techniques*, 4(3), 571-581.

Saleh, R., Shihadeh, A., and Khlystov, A. (2011). "On transport phenomena and equilibration time scales in thermodenuders." *Atmospheric Measurement Techniques*, 4(3), 571-581.

Saleh, R., Khlystov, A., and Shihadeh, A. (2012). "Determination of evaporation coefficients of ambient and laboratory-generated semivolatile organic aerosols from phase equilibration kinetics in a thermodenuder." *Aerosol Science and Technology*, 46(1), 22-30.

Saleh, R., Shihadeh, A., and Khlystov, A. (2009). "Determination of evaporation coefficients of semi-volatile organic aerosols using an integrated volume—tandem differential mobility analysis (IV-TDMA) method." *J. Aerosol Sci.*, 40(12), 1019-1029.

Saxena, P., Hildemann, L. M., McMurry, P. H., and Seinfeld, J. H. (1995). "Organics alter hygroscopic behavior of atmospheric particles." *Journal of Geophysical Research: Atmospheres* (1984–2012), 100(D9), 18755-18770.

Seinfeld, J. H., and Pandis, S. N. (2012). *Atmospheric chemistry and physics: from air pollution to climate change*. John Wiley & Sons, .

Shiraiwa, M., Zuend, A., Bertram, A., and Seinfeld, J. H. (2013). "Gas-particle partitioning of atmospheric aerosols: Interplay of physical state, non-ideal mixing and morphology." Phys.Chem.Chem.Phys., .

Sitariski, M., and Nowakowski, B. (1979). "Condensation rate of trace vapor on Knudsen aerosols from the solution of the Boltzmann equation." J.Colloid Interface Sci., 72(1), 113-122.

Somorjai, G., and Lester, J. (1967). "Evaporation mechanism of solids." Progress in Solid State Chemistry, 4 1-52.

Tolocka, M. P., Jang, M., Ginter, J. M., Cox, F. J., Kamens, R. M., and Johnston, M. V. (2004). "Formation of oligomers in secondary organic aerosol." Environ.Sci.Technol., 38(5), 1428-1434.

Vaden, T. D., Imre, D., Beránek, J., Shrivastava, M., and Zelenyuk, A. (2011). "Evaporation kinetics and phase of laboratory and ambient secondary organic aerosol." Proceedings of the National Academy of Sciences, 108(6), 2190-2195.

Virtanen, A., Joutsensaari, J., Koop, T., Kannosto, J., Yli-Pirilä, P., Leskinen, J., Mäkelä, J. M., Holopainen, J. K., Pöschl, U., and Kulmala, M. (2010). "An amorphous solid state of biogenic secondary organic aerosol particles." Nature, 467(7317), 824-827.

Williams, M., Barrowcliffe, R., Laxen, D., and Monks, P. (2011). "Review of Air Quality modelling in Defra." .

Ziemann, P. J., and Atkinson, R. (2012). "Kinetics, products, and mechanisms of secondary organic aerosol formation." Chem.Soc.Rev., 41(19), 6582-6605.

Zobrist, B., Marcolli, C., Pedernera, D., and Koop, T. (2008). "Do atmospheric aerosols form glasses?" Atmospheric Chemistry and Physics, 8(17), 5221-5244.